

Fuel Plate Deformation Resulting from Fuel Swelling and Aluminum Cladding Constraint

GTRI – Reactor Conversion Program

WBS 21.2.96.2.7 – Out-of-Pile Testing and Codes

Task 13.4.1, Deliverable 1

Nuclear Engineering Division

About Argonne National Laboratory

Argonne is a U.S. Department of Energy laboratory managed by UChicago Argonne, LLC under contract DE-AC02-06CH11357. The Laboratory's main facility is outside Chicago, at 9700 South Cass Avenue, Argonne, Illinois 60439. For information about Argonne and its pioneering science and technology programs, see www.anl.gov.

Availability of This Report

This report is available, at no cost, at <http://www.osti.gov/bridge>. It is also available on paper to the U.S. Department of Energy and its contractors, for a processing fee, from:

U.S. Department of Energy
Office of Scientific and Technical Information
P.O. Box 62
Oak Ridge, TN 37831-0062
phone (865) 576-8401
fax (865) 576-5728
reports@adonis.osti.gov

Disclaimer

This report was prepared as an account of work sponsored by an agency of the United States Government. Neither the United States Government nor any agency thereof, nor UChicago Argonne, LLC, nor any of their employees or officers, makes any warranty, express or implied, or assumes any legal liability or responsibility for the accuracy, completeness, or usefulness of any information, apparatus, product, or process disclosed, or represents that its use would not infringe privately owned rights. Reference herein to any specific commercial product, process, or service by trade name, trademark, manufacturer, or otherwise, does not necessarily constitute or imply its endorsement, recommendation, or favoring by the United States Government or any agency thereof. The views and opinions of document authors expressed herein do not necessarily state or reflect those of the United States Government or any agency thereof, Argonne National Laboratory, or UChicago Argonne, LLC.

Fuel Plate Deformation Resulting from Fuel Swelling and Aluminum Cladding Constraint

GTRI – Reactor Conversion Program

WBS 21.2.96.2.7 – Out-of-Pile Testing and Codes

Task 13.4.1, Deliverable 1

prepared by

Yeon Soo Kim and Gerard L. Hofman

Nuclear Engineering Division, Argonne National Laboratory

June, 2013

This work is sponsored by the U.S. Department of Energy,
National Nuclear Security Administration Office of Global Threat Reduction (NA-21)

In the post-irradiation examination (PIE) of fuel plates, it is a common observation that the fuel meat or foil swelling close to the side rails of the plates is significantly diminished. This phenomenon is clearly observable in some RERTR plates where one of the plate width ends faces the ATR core, resulting in a large power peaking at the foil end and subsequently a peak in fission density (see Fig. 1).

The most plausible causes for this phenomenon are lateral fuel transport toward the fuel center in the width direction and accumulation of fuel mass at regions away from the foil end. The driving force for the fuel volume transport is the shear stress that builds up because of fission product induced fuel swelling and Al cladding strain. Because the plate end is blocked by the cladding and rigid rail, resulting stress directs fuel volume transport away from the fuel end accumulation at a lower stress region toward the fuel width center (Fig. 1). Fission induced creep of U-Mo is the rate controlling mechanism behind this phenomenon [2].

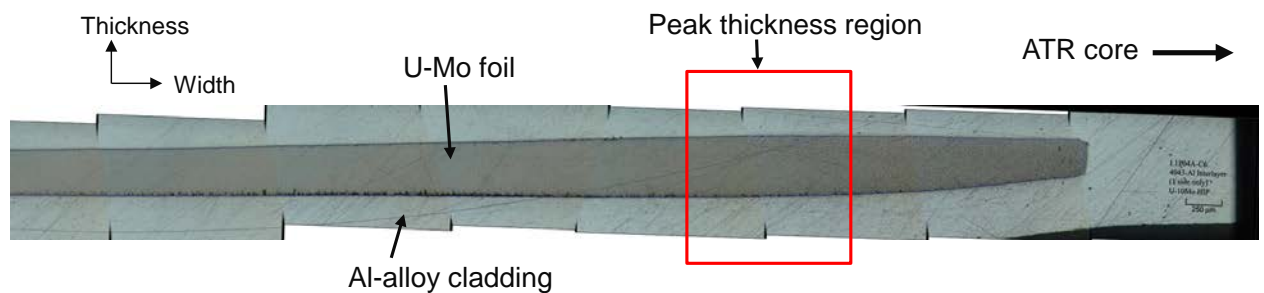


Fig. 1 Fuel plate cross section in the width direction at near the ATR-core side end of L1P04A.

Although similar observations have been made for dispersion fuel plates, it is more difficult to quantify in this type of fuel because of its complex microstructure that includes variations in fuel volume fraction in the meat, the presence of variable fractions of fuel-Al matrix interdiffusion products and pore formation in matrix in some cases. Monolithic foil fuel plates do not have these complications, so this work focuses on analyzing monolithic fuel plates, leaving dispersion fuel plate analysis for future work.

Finite element analysis (FEA) using a commercial code ABAQUS [3] was employed to examine whether the observed phenomenon is physically realistic by applying materials physical-mechanical parameters in reasonable ranges. Simultaneously, another objective of the

FEA simulation was to obtain a creep rate coefficient that enables the extent of the fuel mass transport observed at the end of life (EOL) of the samples caused by creep.

2. Experimental

The samples used for this work were from irradiation tests RERTR-6, -7, -8, -9A, -9B, -10 and -12. The sample fabrication and irradiation properties are summarized in Table 1. The plate dimensions are 100 mm in length, 25 mm in width, and 1.40 mm in thickness, which are a miniature version of full-size fuel plates used in research reactors and test reactors. The fuel foil dimensions are 82.6 mm in length and 19.0 mm in width. Foil thickness is typically 0.25 mm, and in some cases 0.50 mm is used.

The fuel foil is metallurgically bonded to Al 6061 cladding. Two kinds of bonding method were applied. One is friction stir welding (FSW) and - as the name implies - it achieves a metallurgical bonding between the fuel foil and cladding by welding, in which cladding is instantaneously melted at the foil-cladding interface. The other method is hot isostatic pressing (HIP), in which an isostatic pressure of ~103 MPa is applied while the plate is heated at 560 – 580°C for 90 min. The details of the bonding methods can be found, for example, in Ref. [4]. It is worth noting that both bonding methods produce uniform bonding and, more importantly, do not alter foil thickness during the bonding processes.

The fuel plate samples were irradiated in the Advanced Test Reactor (ATR) at INL. The fission rate histories of samples are compared in Fig. 2. One representative sample from each test campaign is included.

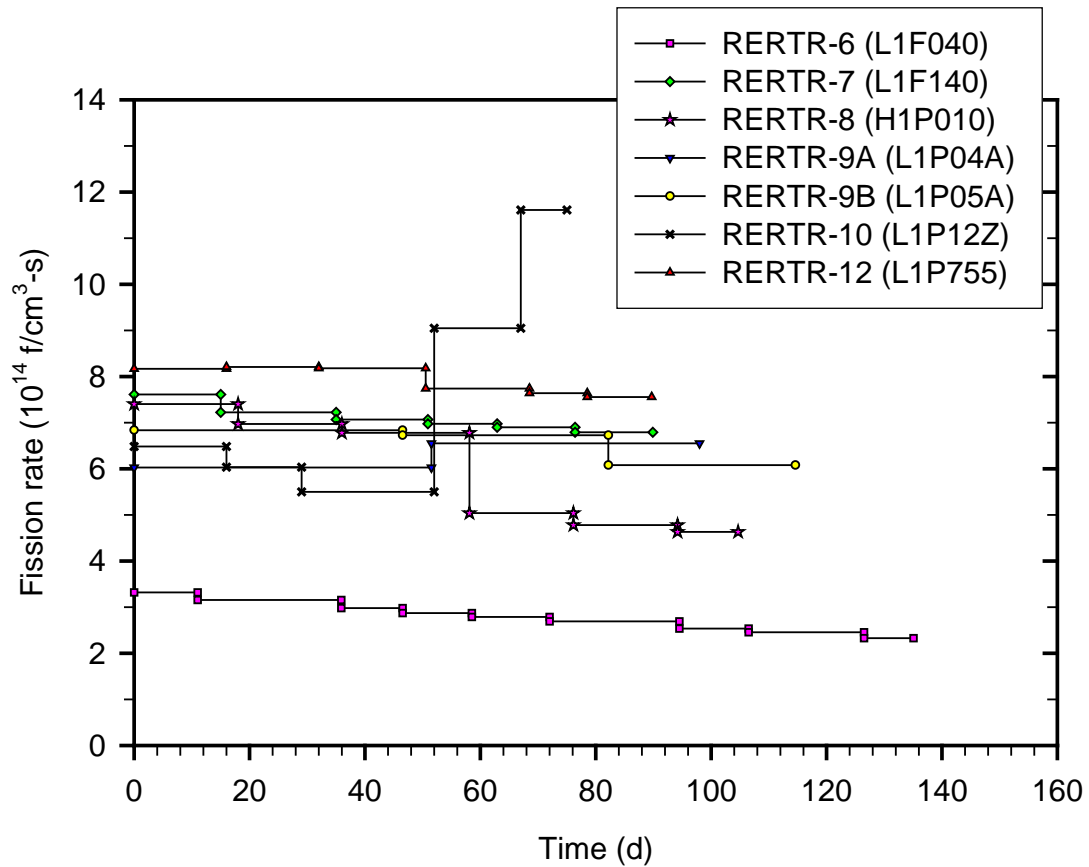


Fig. 2 Foil-averaged fission rate histories of samples. A representative sample from each test is shown. An axial power peaking of 0.95 was multiplied to obtain the real value at the location where the PIE was performed except for RERTR-6. For RERTR-6, the axial power factor is about 1.

The samples were loaded in the ATR in the manner that either a flat surface or a narrow edge faces the ATR core center. In the former case, called face-on loading, the power of the sample in the width direction is approximately symmetric and more uniform. Slight power peakings at the ends still exist due to the self-shielding effect. In the latter case, edge-on loading, the fission density of one edge of the sample that is closer to the ATR core is higher, as is illustrated in Fig. 3. The power ratio of the high power edge to the low power edge is about 2.5 for HEU samples and about 2 for LEU samples (RERTR-6 plates), as determined in neutron physics analyses [5], [6].

After irradiation, the samples were sectioned at the axial mid-plane. The fuel cross section was metallographically examined as shown in Fig. 3.

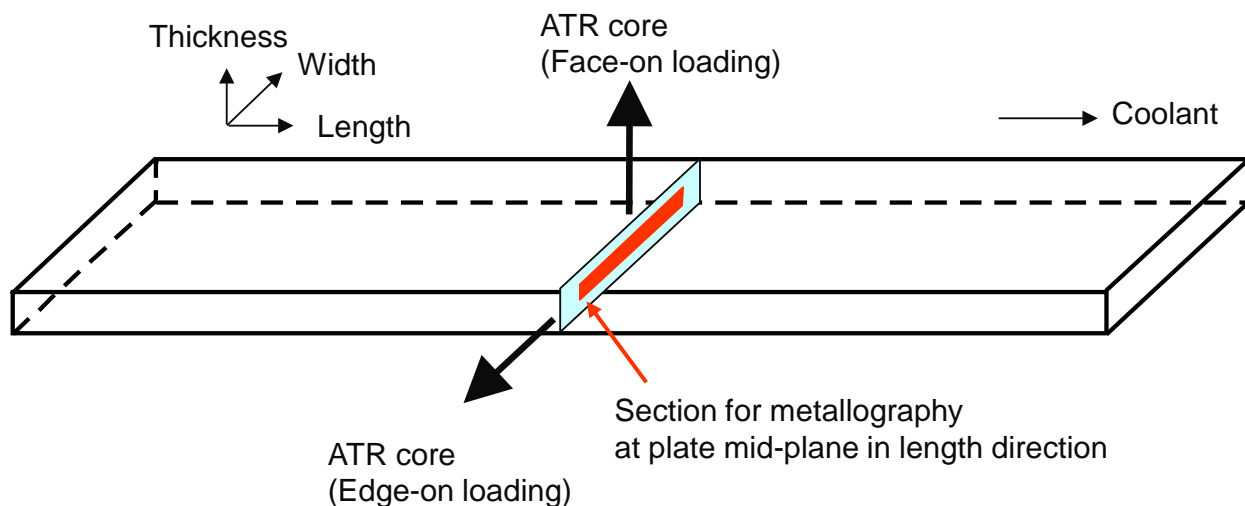


Fig. 3 Schematics of plate loading directions and PIE location

Table 1. Description of irradiation samples used in the analysis

Test	Plate ID	U-Mo foil property and plate fabrication method ^a	Enrichment (%U-235)	U-235 burnup, U-235-fissioned/U-235-initial (%)	Total duration (EFPD)	Fission density (10^{21} f/cm ³) ^b	BOL Fuel Temp (°C) ^c
RERTR-6	L1F040	U-10Mo(f,n)	19.7	46	135	3.0	113
RERTR-6	L1F100	U-10Mo(f,n)	19.7	46	135	3.0	124
RERTR-6	L2F030	U-10Mo(f,t)	19.7	40	135	2.6	145
RERTR-7	L1F140	U-10Mo(f,n)	58.2	27	90	4.4	177
RERTR-7	L2F040	U-10Mo(f,t)	58.3	17	90	2.7	199
RERTR-8	H1P010	U-12Mo(p,n)	57.5	31	105	5.7	164
RERTR-9A	L1P04A	U-10Mo(p,n)	58.3	28	98	4.5	152
RERTR-9A	L1F26C	U-10Mo(f,n)	57.5	33	98	5.5	181
RERTR-9A	L1F32C	U-10Mo(f,n)	57.8	32	98	5.4	181
RERTR-9B	L1F34T	U-10Mo(f,n)	58.8	37	115	6.4	186
RERTR-9B	L1P05A	U-10Mo(p,n)	58.3	34	115	5.5	170
RERTR-9B	L1P09T	U-10Mo(p,n)	58.8	39	115	6.8	189
RERTR-10	L1P12Z	U-10Mo(p,n)	67.0	22	75	4.9	167
RERTR-12	L1P755 ^d	U-10Mo(p,n)	70.0	25	90	5.9	156

a: Number in front of Mo stands for Mo alloying content in weight%.

b: Fuel volume average at EOL including fissions by Pu produced during irradiation.

c: at fuel width center

d: face-on loading. All other samples were edge-on loaded to the center of the ATR (Fig.4).

f: friction bonding

p: hot isostatic pressing bonding

n: as-fabricated foil thickness=0.25 mm, plate thickness = 1.4 mm

t: as-fabricated foil thickness=0.50 mm, plate thickness = 1.4 mm

3. Post-irradiation analysis

As mentioned earlier, fuel swelling in a sample results only in a plate thickness increase because the cladding is relatively unrestrained in the thickness direction. Therefore, once the post-irradiation foil thickness is known, total fuel swelling can be quantified using the following equation:

$$\left(\frac{\Delta V}{V_0}\right)_f = \frac{\Delta t^f}{t_0^f} \quad (1)$$

where Δt^f is foil thickness change after irradiation, and t_0^f is the as-fabricated foil thickness.

For samples from RERTR-6, -7, -8, -9A, 9B, -10 and -12, foil thicknesses were measured using post-irradiation micrographs across the foil width with an interval typically of 0.5 mm. The measured fuel swelling data are given in Table 2. The uncertainty in the measured fuel swelling is $\pm 2\%$, mainly due to the fabrication variability in foil thickness.

Fuel swelling was also calculated by using the correlation available in the literature [1] and comparing it to measurement. Once the fission density at the desired point is known, fuel swelling can be calculated using the correlation. However, the calculated fuel swelling is purely by fission products; mass transfer by creep is not included. The calculated fuel swelling values are also included in Table 2.

The measured fuel swelling data of L1P04A are plotted with the calculated in Fig. 4. The measured swelling at the tapered end of the foil, marked by A in Fig. 4, is substantially lower than the calculated value. In fact, it is even lower than the fuel swelling by solid fission products only. This and the evidence that the fission gas porosity does not vary appreciably along several millimeters from the foil end (see Fig. 5) rule out, at least to the first order, the effect of fission gas induced fuel swelling, per se. A and B, the areas enclosed by the measured fuel swelling curve and the calculated swelling curve, are the same magnitude. The similar observation is also made for C and D at the opposite end of the foil end. This salient phenomenon is commonly observed for all samples, although area comparisons are not perfectly consistent in some samples. The conclusion is that a mass transfer has occurred from A to B, facilitated by fission induced creep in the fuel as a response to an applied stress.

Table 2. Fuel swelling comparison between measured and calculated, $\left(\frac{\Delta V}{V_0}\right)_f$ (%)

Distance from foil end (mm) ^a		0	0.5	1	1.5	2	2.5	3	3.5	4	4.5	5	5.5	6	6.5	7	7.5	8	8.5	9	9.5
L1F040	M	0	7	17	22	28	29	28	25	23	21	21	19	19	19	19	17	17	16	16	15
	C	21	19	19	18	17	16	16	15	15	14	14	14	13	13	13	12	12	12	12	12
L1F100	M	0	10	17	26	31	31	31	29	27	21	25	23	23	22	17	19	19	18	18	16
	C	26	25	24	23	22	21	21	20	19	19	18	18	17	17	17	17	17	16	16	15
L2F030	M	0	8	14	20	24	24	22	20	18	17	16	15	14	13	13	13	12	12	12	11
	C	17	16	16	15	14	14	14	13	13	12	12	12	12	11	11	11	11	10	10	10
L1F140	M	0	28	45	55	59	60	56	48	42	38	35	33	30	30	29	29	27	27	25	24
	C	65	58	52	48	45	42	40	38	36	34	33	32	30	29	28	27	26	26	25	24
L2F040	M	0	9	18	25	29	30	29	26	24	22	21	20	20	19	19	19	17	17	17	16
	C	35	31	28	26	25	23	22	21	20	19	18	18	17	16	16	15	15	15	14	14
H1P010	M	0	23	45	60	70	70	70	60	60	53	50	48	45	43	40	40	38	38	38	38
	C	75	67	61	55	52	49	47	44	42	40	39	39	37	35	34	32	32	31	30	29
L1P04A	M	0	20	45	56	63	64	63	59	52	45	38	35	33	31	30	29	27	26	25	23
	M ^b	0	11	21	26	28	30	29	27	24	23	23	22	21	21	21	21	21	21	22	23
	C	71	65	59	54	49	45	42	39	37	35	33	32	31	29	28	28	27	26	25	25
	C ^b	21	21	20	20	20	20	20	20	20	20	21	21	21	22	22	23	23	24	24	25
L1F26C	M	2	18	37	57	70	74	76	75	71	65	57	53	49	45	41	37	36	35	34	33
	C	76	68	63	59	56	53	50	48	46	44	42	40	39	38	37	36	34	34	33	32
L1F32C	M	0	21	42	58	70	75	77	75	71	62	55	50	45	42	39	37	35	33	32	32
	C	72	67	62	58	54	51	48	46	44	42	40	39	38	36	35	35	34	33	32	32
L1F34T	M	0	25	46	64	77	80	80	76	73	68	63	57	52	50	47	45	42	40	40	39
	C	98	89	82	76	70	66	62	58	55	53	51	49	47	46	44	43	42	41	40	39
L1P05A	M	0	21	42	56	67	71	73	73	69	63	58	52	48	44	42	39	37	35	33	32
	M ^b	0	13	25	31	32	33	32	31	30	29	29	28	28	28	29	30	30	31	31	32
	C	91	81	73	67	62	58	55	52	49	47	45	43	41	40	39	37	36	35	34	33
	C ^b	28	27	27	27	27	27	27	27	27	27	27	28	28	28	29	30	30	31	34	33
L1P09T	M	5	37	64	76	88	90	88	86	80	74	70	66	62	60	56	49	47	45	43	41
	C	104	95	87	81	75	70	66	63	60	57	55	53	51	50	48	47	46	45	44	43
L1P12Z	M	8	30	52	61	68	62	58	53	47	43	37	37	33	31	28	25	25	22	22	20
	M ^b	0	7	16	21	21	21	20	18	18	18	19	18	19	19	20	21	21	21	21	20
	C	72	65	59	54	49	46	42	40	37	35	33	32	31	29	28	28	27	26	25	25
	C ^b	21	21	20	20	20	20	20	20	20	20	21	21	21	22	22	23	23	24	24	25
L1P755	M	15		45		52		43		37		32		30		27		26		25	
	M ^c	12		38		42		38		28		27		25		25		25		24	
	C	50		43		38		35		32		30		29		28		27		27	
	C ^c	42		36		31		29		27		26		26		26		26		26	

M: Measured

C: Calculated

a: Distance from higher power side of foil end

b: Distance from lower power side of foil end

c: Distance from the opposite end of the foil in the face-on loaded sample

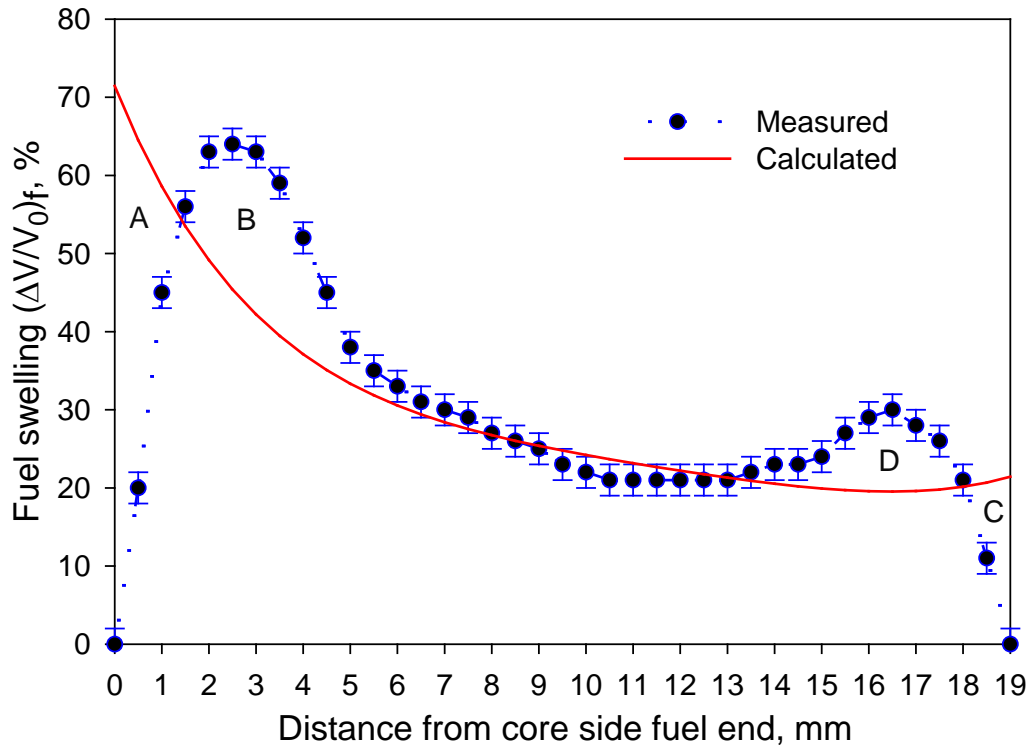


Fig. 4 Fuel swelling comparison between measured and calculated for L1P04A.

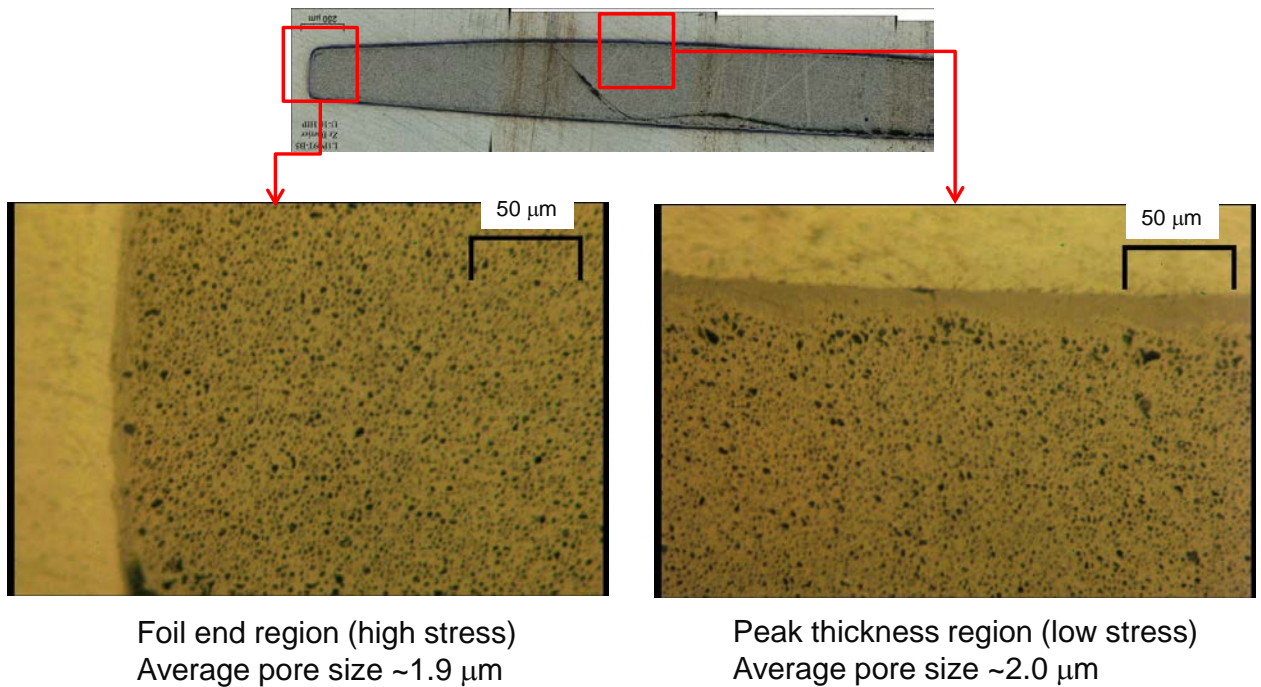


Fig. 5 Optical micrographes showing fission gas pore morphology of L1P09T.

4. ABAQUS simulation

4.1. Input data

Young's modulus of 66 GPa and Poisson's ratio of 0.34 for AA6061 cladding are taken from Ref.[7]. Yield strength of the tempered Al alloys increases to ~280 MPa due to irradiation hardening [1]. This datum is used for AA6061 cladding considering fabrication and post-fabrication processes. Strain hardening of the Al-alloy cladding is taken into account. The strain hardening exponent of 0.13 for AA6061-T6 [9] is applied to cladding with consideration of a decreased potential of strain hardening by neutron irradiation.

Young's modulus of U-Mo fuel of 85 GPa and Poisson's ratio of 0.34 are used for U-Mo alloy [8]. Yield strength of U-Mo is not needed in the simulation.

Fission-induced creep of U-Mo is dependent on the applied stress and fission rate. The following equation can be used to express the extent of U-Mo creep:

$$\dot{\epsilon}_c = A \sigma \dot{f} \quad (2)$$

where $\dot{\epsilon}_c$ is the equivalent creep strain rate (s^{-1}), A the creep rate coefficient (cm^3/MPa), σ the equivalent stress (MPa), and \dot{f} the fission rate (fissions/ cm^3 -s). Thermal creep is not considered because the temperature regime of interest is so low that this phenomenon is inactive.

The fuel swelling correlation from Ref. [1] is adopted:

$$\left(\frac{\Delta V}{V_0}\right)_f = 5.0 f_d, \quad \text{for } f_d \leq 3 \times 10^{21} \text{ fissions/cm}^3 \quad (3)$$

$$\left(\frac{\Delta V}{V_0}\right)_f = 15 + 6.3(f_d - 3) + 0.33(f_d - 3)^2, \quad \text{for } 3 \times 10^{21} < f_d \text{ fissions/cm}^3 \quad (4)$$

where fuel swelling is in percent and f_d is in $10^{21} f/cm^3$. Note that the temperature effect is not considered in these equations for the following reasons. At the low temperature regime below ~250 °C, fission gas diffusion is predominantly by fission enhanced diffusion (FED) and thermally activated gas diffusion is small.

Fuel true strain is obtained by converting fission product induced fuel swelling given in Eqs. (3) and (4) as follows:

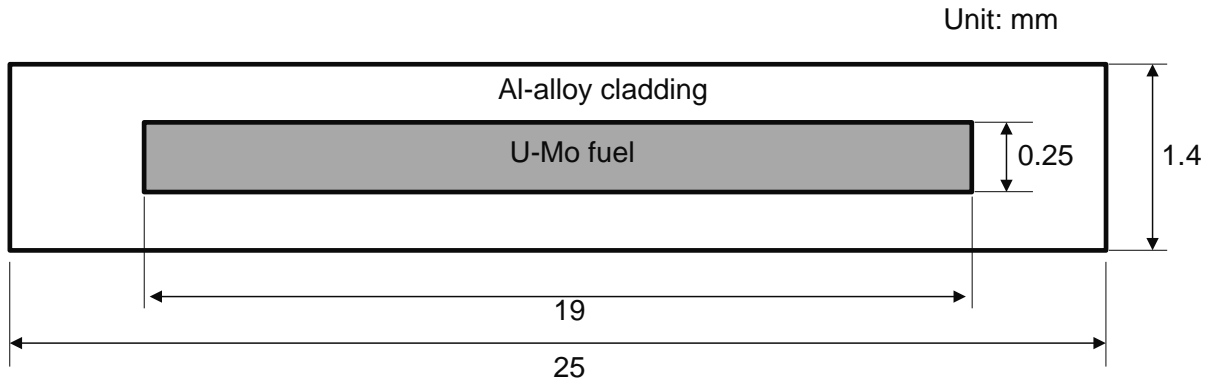
$$\varepsilon_{f,true} = \ln \left[1 + \left(\frac{\Delta V}{V_0} \right)_f \right] \quad (5)$$

4.2. Simulation for creep rate coefficient

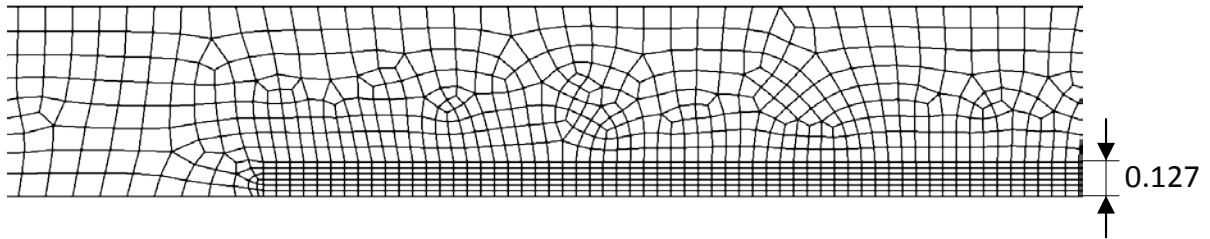
The creep rate coefficient A in Eq. (2) is obtained by simulation of the U-Mo creep using ABAQUS FEA simulation.

The EOL condition of the plate L1P04A, which was irradiated with edge-on loading and has the same cladding thickness on both faces, was simulated. For this case, only the upper half of the fuel plate was modeled by symmetry. A schematic of fuel plate cross-section and the FEA modeling scheme are shown in Fig. 6.

CPEG8R, generalized plane strain 8-node quadratic element with reduced integration, is used. A geometrically nonlinear analysis is applied to make more precise analysis based on the geometry in the most recently completed increment. Again, bonding between fuel and cladding is assumed intact throughout life, which is inaccurate in some cases where debonding occurs.



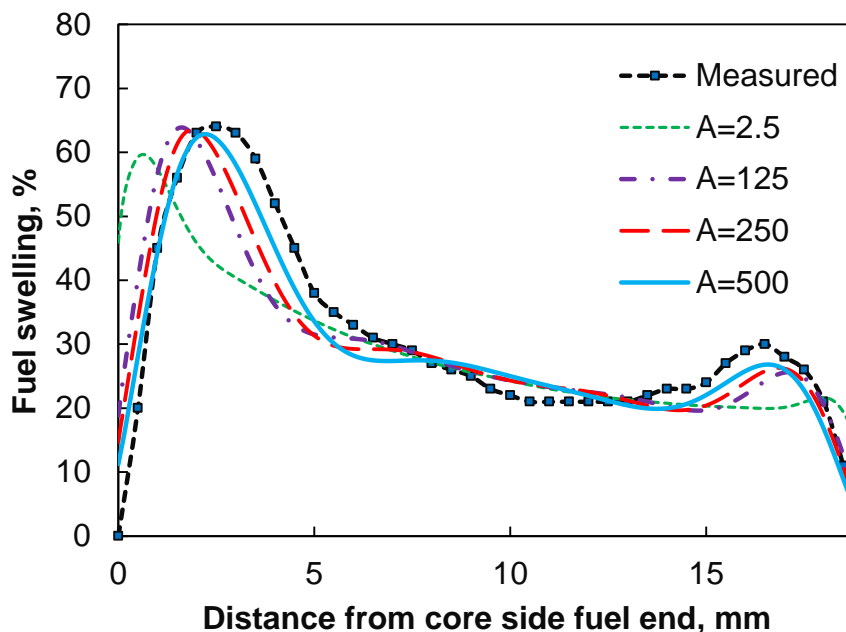
(a) Schematic of fuel plate cross section



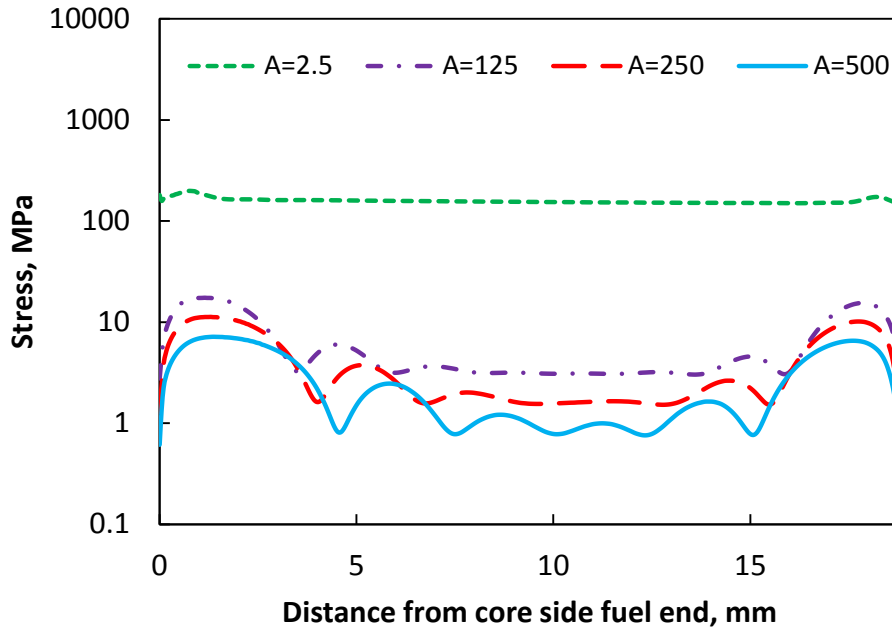
(b) Finite element modeling

Fig. 6 Finite element modeling for L1P04A with edge-on loading and symmetric cladding thickness.

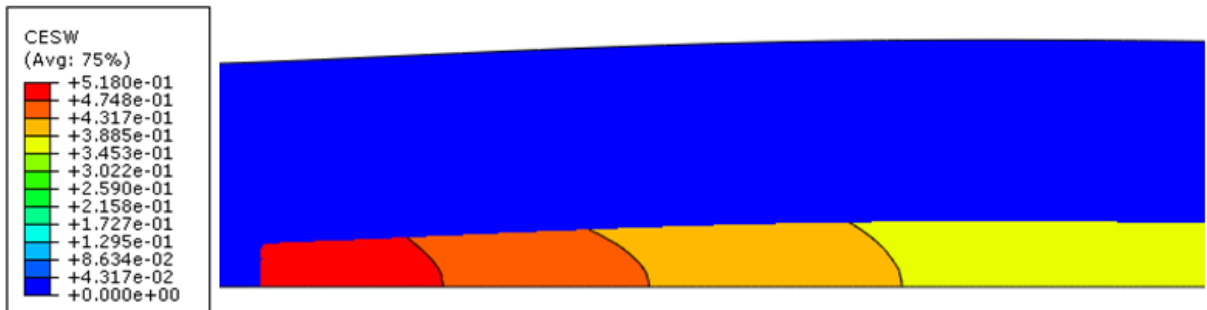
FEA simulation was performed for fission product induced fuel swelling together with creep in L1P04A using several A values, and the best simulation was found when $A = 500 \times 10^{-25} \text{ cm}^3/\text{MPa}$, as shown in Fig. 7. The fuel swelling simulation plotted in Fig. 7(a) shows fair simulation of the swelling peaks at both fuel ends. As the creep coefficient increases, the peaks move toward the foil width center, and their apices become closer to the measured. Fitting becomes worse again when A is increased greater than $A = 500 \times 10^{-25} \text{ cm}^3/\text{MPa}$. However, the uncertainties involved in the fuel swelling and the small difference from the case with $A = 250 \times 10^{-25} \text{ cm}^3/\text{MPa}$ suggest that the obtained creep rate constant should also include considerable uncertainty although it is difficult to quantify.



(a) Fitting fuel swelling for creep rate coefficient by comparing with the measured. A is in $10^{25} \text{ cm}^3/\text{MPa}$.



(b) Von Mises stress corresponding to the creep rate coefficient given in (a).



(c) Contour of fuel volume expansion by the combination of fuel swelling and creep-induced mass transfer from the foil end region to the foil central region

Fig. 7 Finite element simulation results to fit creep rate coefficient using the measured data for L1P04A.

The corresponding Von Mises stresses for the fuel swelling given in Fig. 7(a) are plotted in Fig. 7(b). It is considered that the stresses obtained with $A = 500 \times 10^{-25} \text{ cm}^3/\text{MPa}$ is reasonable. The stress becomes zero at the foil end to satisfy the traction free boundary condition. It is also worth noting that the stress at the fuel central region in the width direction becomes smallest. The wave nature in stress suggests that this uneven stress state may be the

major driving force to cause separation of fuel foil from cladding during irradiation observed in some plates.

The simulation result of the combination of fission product induced fuel swelling and fuel mass transfer from the foil end to the foil central region in L1P04A is shown in Fig. 7(c). The FEA simulation also implies that fuel volume increase by fission product-induced fuel swelling at the foil end region is effectively removed and accumulate instead at the region showing peak foil thickness. Fuel flow is the highest at the foil thickness centerline and the lowest at the foil-cladding interface where the fuel is assumed to be perfectly bonded with the cladding.

The driving force for the mass transfer is provided by shear stress in the foil width direction. The evolution of the shear stress at the foil-cladding interface in the thickness direction is calculated at BOL, MOL and EOL and shown in Fig. 8. The shear stress increases as fission product induced fuel swelling increases. As a result, mass transfer increases.

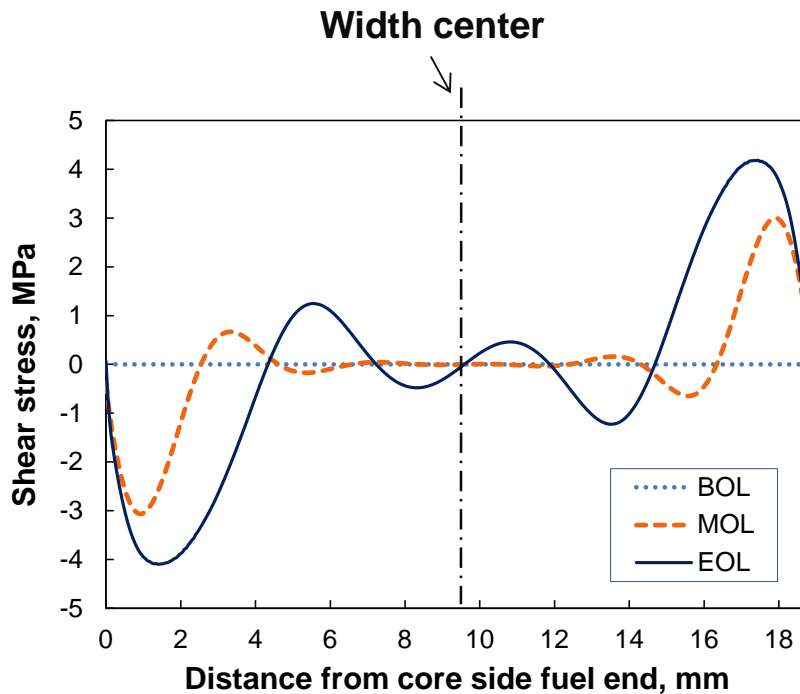


Fig. 8 Calculated shear stress at the foil-cladding interface at three points in irradiation time of L1P04A. The signs are opposite across the center in the width direction due to direction change.

4.3. Validation of FEA simulation

The creep rate coefficient obtained in the previous subsection $A = 500 \times 10^{-25} \text{ cm}^3/\text{MPa}$ and the FEA simulation results are examined by applying this value in simulation for other plates. Among the measured plates given in Table 2 three plates with different fabrication geometry and plate loading direction are selected.

L1P04A is a plate having symmetric cladding thickness on both plate sides and edge-on loaded. L1P05A is a similar sample as L1P04A. FEA simulation was performed for L1P05A using the same creep rate coefficient, $A = 500 \times 10^{-25} \text{ cm}^3/\text{MPa}$. The FEA result is in reasonable agreement with the measurement (Fig. 9), although the simulated apex at the core side of L1P05A exhibits a slight discrepancy with the measurement.

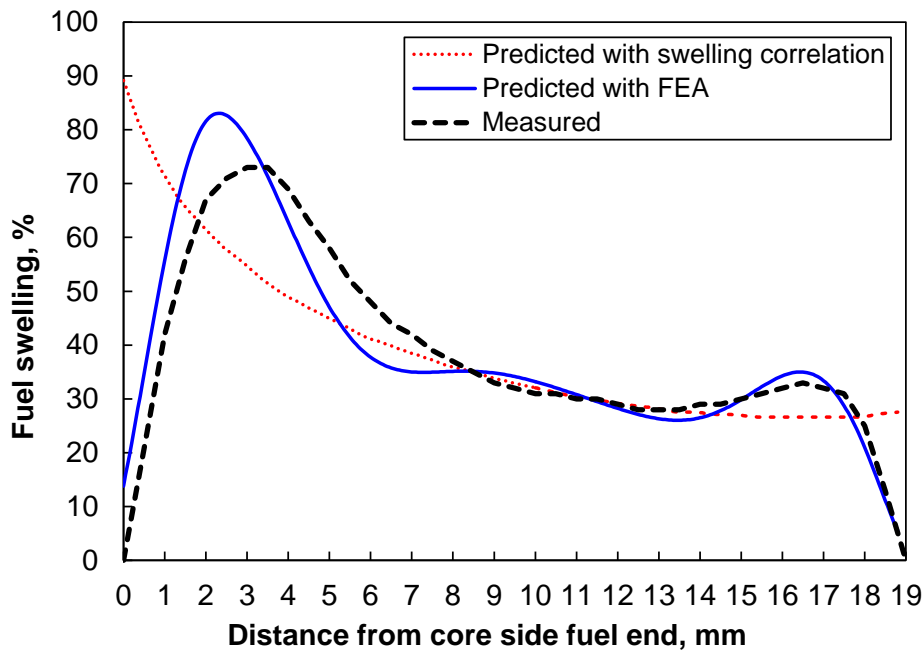
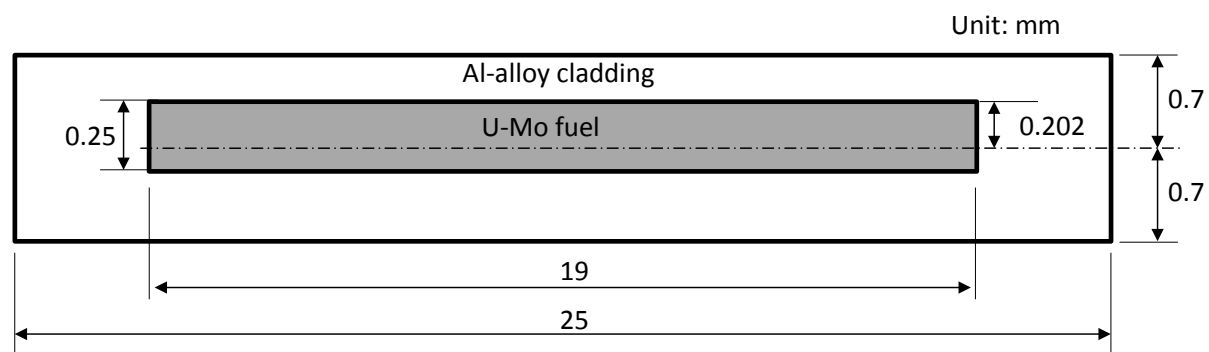


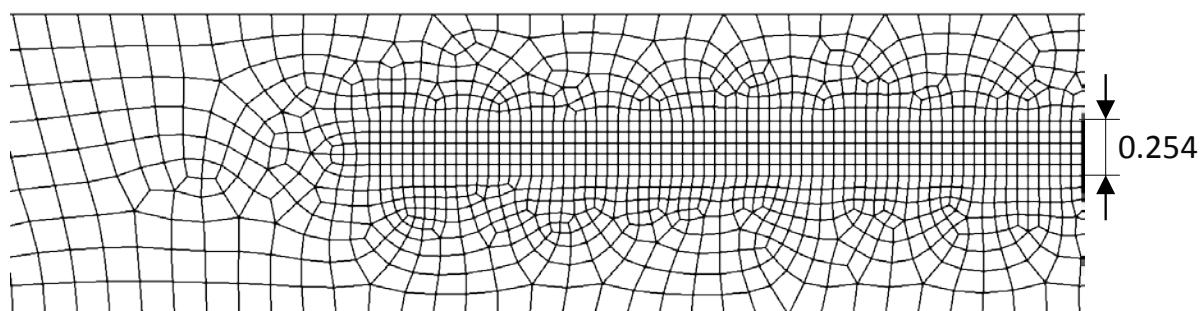
Fig. 9 Comparison of the predicted fuel swelling by FEA to the measured of L1P05A. The predicted fuel swelling by empirical correlation is also provided as reference.

L1P12Z was inadvertently fabricated with different cladding thickness on each side (see Fig. 10). FEA simulation was made for L1P12Z, using $A = 500 \times 10^{-25} \text{ cm}^3/\text{MPa}$, to include the effect of the asymmetric cladding thickness. The schematic of fuel cross section and the fuel Fig. 11(a), the FEA result is in excellent agreement with the measured for fuel swelling. Fuel

deformation obtained by FEA shown in Fig. 11(b) occurs dominantly on the thin cladding side of the plate compared to the thick side, which is in accord with the metallography shown in Fig. 11(c).

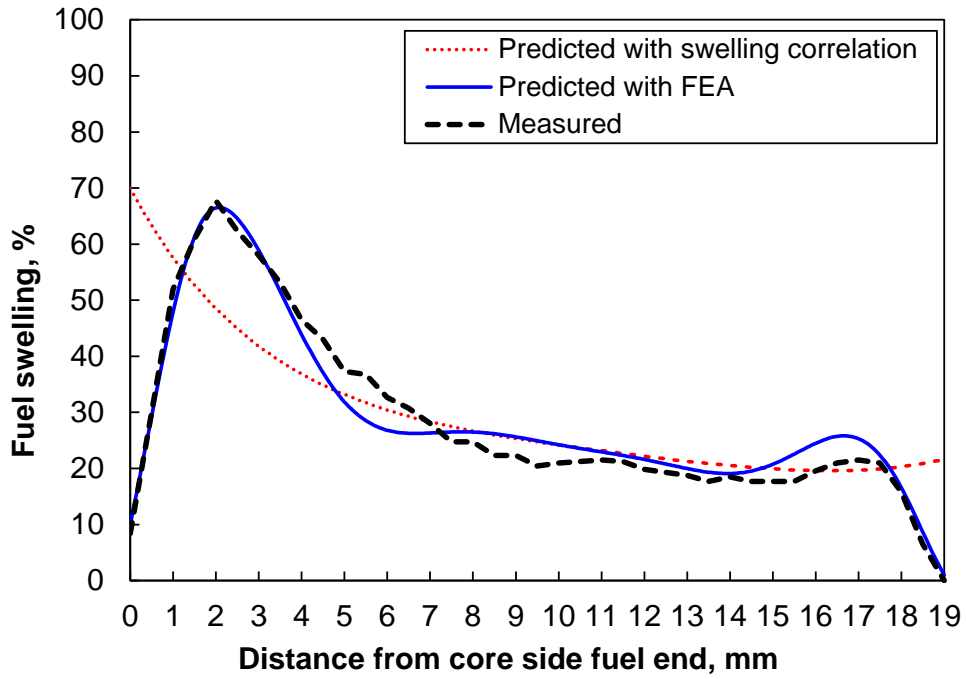


(a) Schematic of fuel plate cross section

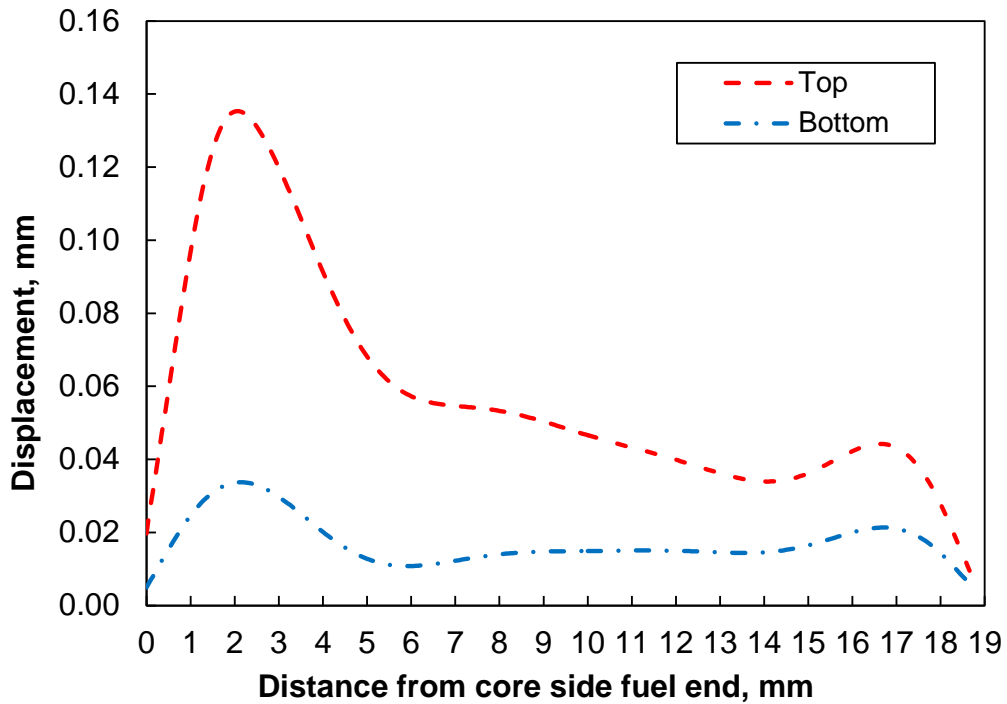


(b) Finite element modeling

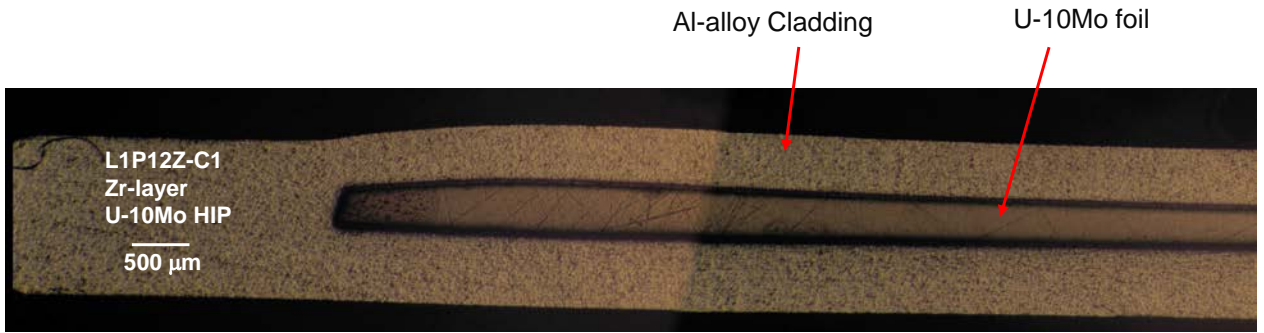
Fig. 10 Finite element modeling for L1P12Z with edge-on loading and asymmetric cladding thickness on each side.



(a) Comparison of the predicted fuel swelling by FEA to the measured of L1P12Z. The predicted fuel swelling by empirical correlation is also provided as reference.



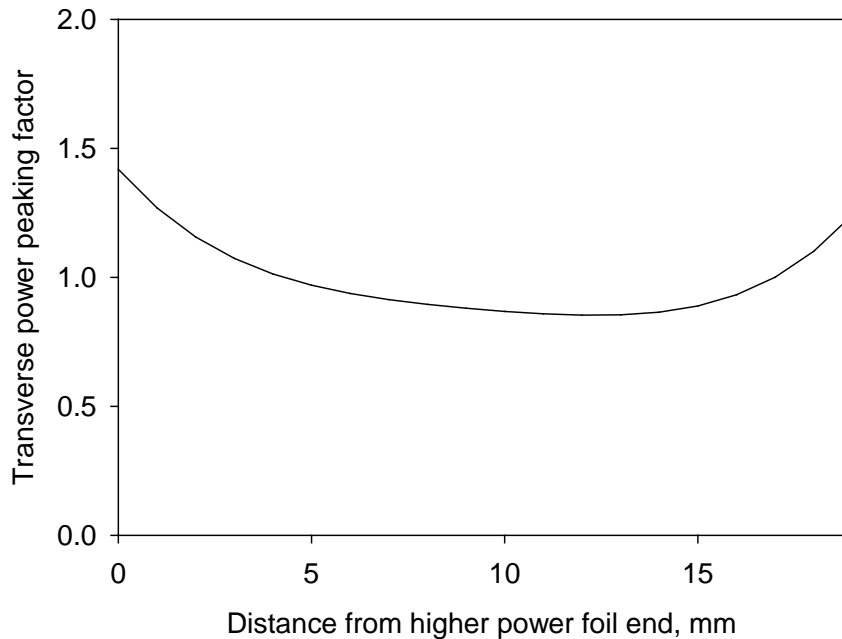
(b) Fuel displacements for both halves of the foil.



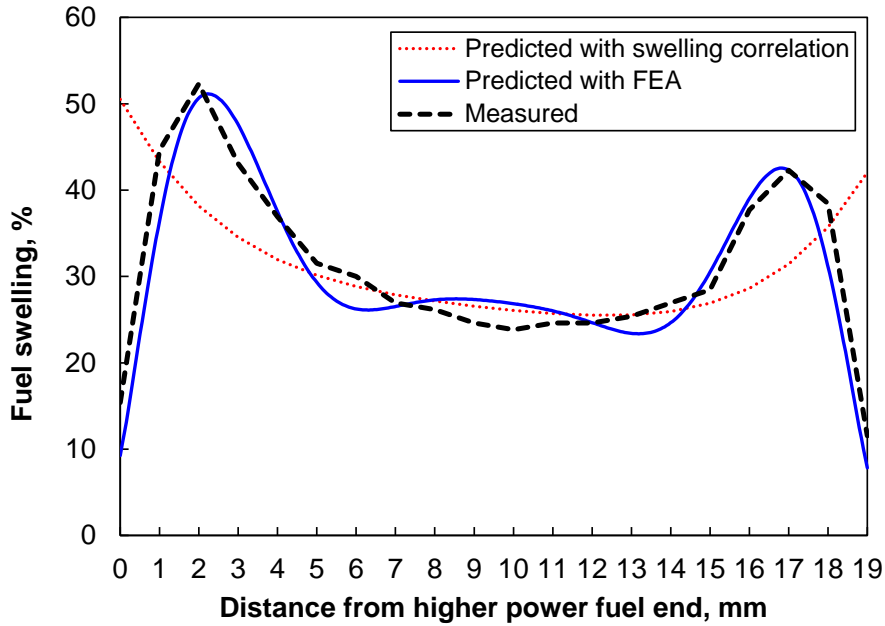
(c) Optical micrograph of cross section of L1P12Z in the width direction. *Note that cladding deformation is confined to thinner cladding.*

Fig. 11 Finite element analysis results and PIE data of L1P12Z.1

L1P755 from the RERTR-12 test is a face-on loaded. This loading scheme was employed to provide a more uniform power distribution across the plate width. However, gamma scanning during post-irradiation examination showed that power peaking still exists although less than the edge-on loaded plates as shown in Fig. 12(a). The FEA simulation result for L1P755, using $A = 500 \times 10^{-25} \text{ cm}^3/\text{MPa}$ shown Fig. 12(b) compares the FEA simulation result with the measured fuel swelling and the calculated fuel swelling without considering creep, in which the FEA simulation is consistent with the measurement.



(a) Power peaking factors in the foil width direction measured by gamma scan



(b) Comparison of the calculated fuel swelling by FEA to the measured. The predicted fuel swelling by empirical correlation is also provided as reference.

Fig. 12 Power distribution across foil width and FEA analysis results for L1P755.

5. Discussion

The consistent FEA simulations with the measured data for L1P05A, L1P12Z and L1P755 using the creep rate coefficient $A = 500 \times 10^{-25} \text{ cm}^3/\text{MPa}$ in general implies that the fuel mass transfer is indeed enabled by a creep mechanism and that ABAQUS FEA is applicable in simulation of the fission induced creep observed for U-Mo alloy fuel regardless of fuel fabrication and loading types. ABAQUS FEA also demonstrates that not only the obtained creep rate constant is acceptable, but also the FEA modeling itself is valid in simulating the measured data.

Fission enhanced creep at low homologous temperatures was reported for all uranium fuels and was first identified in α -U in the 1950s by Russian [12] and British [13] workers, and subsequently in ceramic fuels by various researchers [14]-[21]. Common for all, the creep rate was found to be athermal and have a linear dependence on the applied stress and fission rate, as is the case in Eq. (2). The obtained creep rate coefficient $A = 500 \times 10^{-25} \text{ cm}^3/\text{MPa}$ is compared with other U-fuels in the literature at homologous temperatures relative to their melting points in Table 3. The obtained value lies between values of pure uranium and MOX,

and is about a half of the value of pure U. The slightly lower creep rate of the U-10Mo than pure U is most likely due to the less dense γ -phase (bcc) as compared to the denser α -phase (orthorhombic) in which pure U exists.

Table 3 Creep rate coefficient (A) in Eq. (2)

Fuel	A (10^{-25} cm ³ /MPa)	$\sim T/T_m$	Reference
U	800	0.3	[12], [15]
U-10wt.%Mo	500	0.3	Present study
MOX	56	0.25	[16]
UO ₂	7	0.25	[17],[18],[19]
UN	3	0.3	[20], [21]
UC	1	0.3	[19]

The high creep rate enables the extent of observed fuel lateral mass transfer, which is the effective mechanism that lessens the stresses caused by fission product induced fuel swelling. This mechanism allows U-Mo fuel to achieve high burnup without failure, by reducing the potential to plate buckling due to lateral stresses induced by fuel swelling. The high creep rate can also explain the extent of fuel particle deformation observed in high burnup dispersion fuel plates shown in Fig. 13, in which the spherical U-Mo particles, when they were as-fabricated, underwent significant deformation during irradiation. This sample also shows sintering between particles. The analysis of creep behavior of the dispersion fuel samples is not pursued in this work.

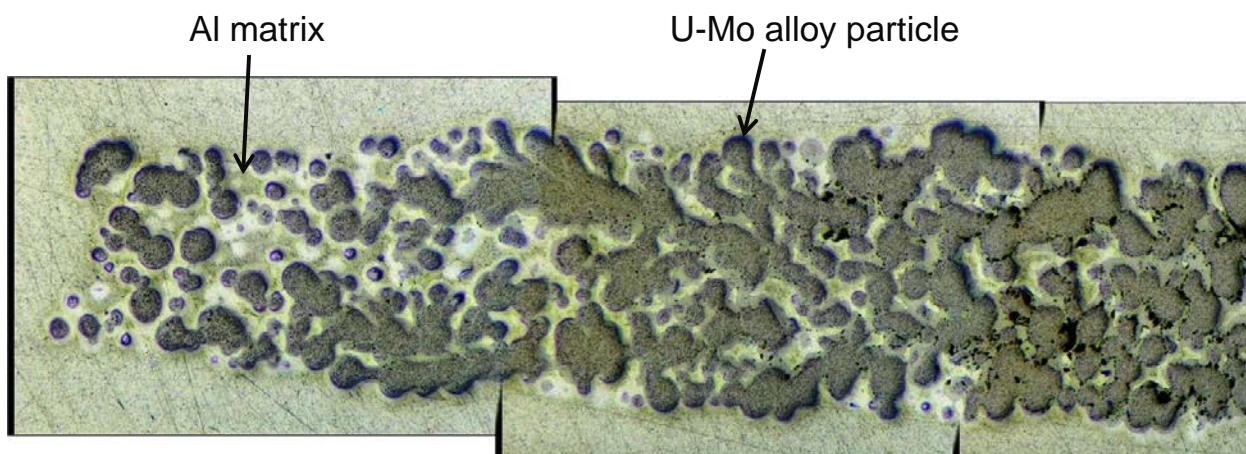


Fig. 13 Optical micrograph of fuel meat end region of R6R018 where the meat-averaged fission density is $\sim 10 \times 10^{21}$ f/cm³-fuel-particle.

The rather large increase in local fuel loading at the peak thickness location resulting from the lateral fuel creep may have to be considered for hot-spot calculations for reactors that operate fuel at high power after substantial burnup. The additional plate thickness increase by creep in addition to fission product induced fuel swelling at the peak thickness location must be incorporated in safety analyses. The additional foil thickness increase by creep is ~25% from the as-fabricated foil thickness at a fission density of $7 \times 10^{21} \text{ f/cm}^3$, which may be considerable in a safety analysis. The cladding deformation profile follows that of the fuel foil and can therefore be rather non-uniform.

In the FEA analyses performed in this study, we used life-averaged fission rates instead of the time-dependent ones given in Fig. 2 for the ease of calculation. The validity of this simplistic approach was examined. Fission induced creep is a product of stress and fission rate; however, the stress is more important because it provides the driving force and the fission rate determines amplitude of the creep rate. The stress is produced by the fission product induced fuel swelling, which is a function of fission density. The total creep strain is a time integration of the creep rate given in Eq. (2). Therefore, the time-dependent fission rate is used, the fission density is inevitably larger than that in the average-fission rate case in early life because the fission rate decreases with burnup in all of the tests, except for RERTR-9A. FEA simulation for L1F140 at middle of life (MOL) compares the two cases in Fig. 14. Fuel swelling was slightly (~2%) larger for the time-dependent fission rate case at peak thickness location, whereas no difference was found at EOL between the two cases. This result is undoubtedly due to the linear stress and fission rate dependence of the creep rate.

Studies of the effect of porosity on thermal creep are available in the literature (see for example [22]). Porosity typically enhances the thermal creep rate. Since fission gas pores are formed in U-Mo, the porosity effect may be important for a more accurate analysis. Porosity in some high burnup U-Mo samples becomes considerable, greater than 10%. Hayes estimated ~12% augmentation in the creep rate was needed at this porosity in UO_2 . Unlike thermal creep, however, for which the exponent of stress term ranges 3 – 4, the porosity effect for fission induced creep is smaller because the exponent for the stress term is one. For this reason, a detailed study to accurately factor this effect is not included in this study.

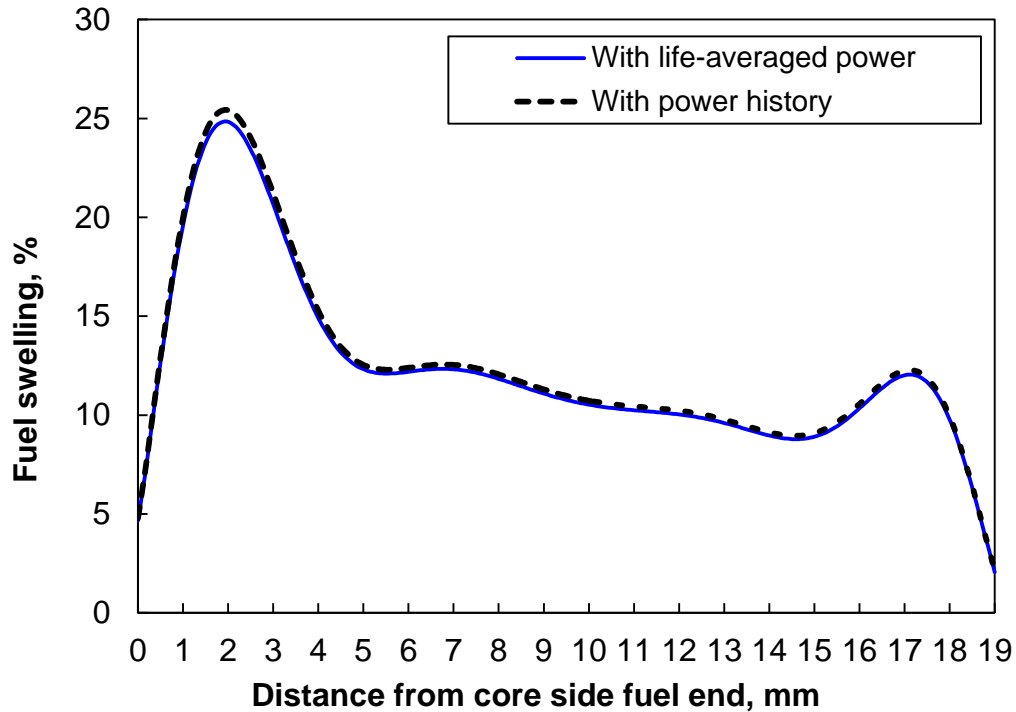


Fig. 14 Comparison of FEA results for fuel swelling between time-dependent fission rate and life-average fission rate at MOL for L1F140.

The temperature effect is not considered in the FEA performed in this study, which follows the findings reported in the literature [12]-[21]. The temperatures of the samples analyzed in this work are narrowly bounded between 110 – 190°C (Table 1). This low and narrow range of temperatures is the prerequisite for athermal creep.

An implication from this work that affects the measurement of fission product induced fuel swelling is that one must avoid measuring it at or near the foil end regions. Measurements at these regions will lead to erroneous results affected by fuel lateral mass transfer.

6. Conclusions

The taper of U-Mo fuel foil observed at the foil width end region, where fission density is highest, has been reviewed. The underlying mechanism is lateral mass transfer by fission induced creep, which is athermal and dependent on fission rate and stress that builds up by fission product induced fuel swelling and the constraint of the Al cladding. This enables the

thin U-Mo alloy fuel plates to achieve high burnup. It also provides a realistic explanation for the observed anisotropic swelling in the fuel plates, as well as the non-uniform cladding strain.

ABAQUS finite element analysis (FEA) simulation coupled with the model for fission product induced fuel swelling and creep produced consistent results using the measured fuel swelling data for all fuel plate types and loading schemes with physical-mechanical data available in the literature. This proves that the fuel mass transfer is indeed induced by a creep mechanism and validates that ABAQUS FEA is applicable in simulation of the fission induced creep observed for U-Mo alloy fuel.

ABAQUS simulation also produced the best-fit creep rate constant for U-10Mo alloy fuel $500 \times 10^{-25} \text{ cm}^3/\text{MPa}$, a value that is approximately a factor of two lower than that for pure uranium. However, the obtained creep rate constant includes considerable uncertainty, for which quantification is not tried in this study.

Acknowledgments

The authors would like to thank Mrs. C. Clark, G. Moore, and J. Jue for the fabrication of the samples used in this work. The operations staff at ATR is also acknowledged for the irradiation tests. The physics data available by Dr. G. Chang and Ms. M. Lillo are also appreciated. A. Robinson is thanked for leading the post-irradiation examination and making the data available to the authors. Authors are grateful to Dr. J.S. Cheon for his ABAQUS analyses and Mr. Y.S. Choo of KAERI for the measurement of pore sizes used in Fig. 6. This work was supported by the U.S. Department of Energy, Office of Global Threat Reduction (NA-21), National Nuclear Security Administration, under Contract No. DE-AC-02-06CH11357 between UChicago Argonne, LLC and the Department of Energy.

References

- [1] Y.S. Kim, G.L. Hofman, J. Nucl. Mater., 419 (2011) 291.
- [2] G.L. Hofman, Y.S. Kim, A.B. Robinson, Trans. 13th Internat. Topical Meeting Research Reactor Fuel Management (RRFM), RRFM 2009, Vienna, Austria, March 22 -25, 2009. <http://www.euronuclear.org/meetings/rrfm2009/index.htm>
- [3] ABAQUS Analysis User's Manual, Dassault Systems, 2011.

- [4] C.R. Clark, J.M. Wight, G.C. Knighton, G.A. Moore, J.F. Jue, the 27th International Meeting on Reduced Enrichment for Research and Test Reactors (RERTR), Boston, Massachusetts, November 6-10, 2005. <http://www.rertr.anl.gov/RERTR27>
- [5] M. A. Lillo, "MCNP-calculated gradients across RERTR-6 and RERTR-7 miniplates irradiated in ATR," Interoffice Memo, INL, 2007.
- [6] G. S. Chang, M. A. Lillo, 2008, "As-Run Neutronics Analysis of the RERTR-9A/B Capsules in the ATR B 11 Position," Engineering Calculations and Analysis Report - 231, 2008.
- [7] J.S. Cheon, Y.S. Kim, Material Properties of Aluminum Alloys and Pure Zirconium for Use in High-density Fuel Development for Research Reactors, ANL/RERTR/TM-12-6, 2012.
- [8] Nomine, A. M., Bedere, D., and Miannay, D., "Grandeur, mecaniques associées à la corrosion sous contrainte de l'alliage U-10Mo," paper presented at the Coloque sur la rupture des materiaux, Grenoble, 9-21 January 1972.
- [9] Y. Tamarin, Atlas of Stress-Strain Curves, Materials Park, Ohio, ASM International, 2002.
- [10] M.L. Bleiberg et al., J. Appl. Phys., 27(11) (1956) 1270.
- [11] M.L. Bleiberg, J. Nucl. Mater., 2 (1959) 182.
- [12] S.T. Konobeevsky, N.E. Pravdyuk, V.I. Kutaitsev, UN Int'l Conf. Peaceful Use of Atomic Energy, Geneva, Switzerland, Paper no. 681, 1955.
- [13] A.C. Roberts, A.H. Cottrell, Phil. Mag., 1 (1956) 711.
- [14] A.S. Zaimovsky, UN Int'l Conf. Peaceful Use of Atomic Energy, 1958.
- [15] M. Hesketh, Discussion in paper: M. Englander, C. T. Montpreville, 11th Colloque de Metallurgie, Creep, June 1967, p.28, Centre D'Etudes Nucleaires de Saclay, 1968.
- [16] R. J. White, The Re-irradiation of MIMAS-MOX Fuel in IFA-629.1, HWR-586, March, 1999.
- [17] A.A. Solomon, J. Am. Ceram. Soc., 56 (1973) 164.
- [18] W. Dienst, J. Nucl. Mater., 65 (1977) 1.
- [19] D.J. Clough, J. Nucl. Mater., 65 (1977) 24.
- [20] D. Brucklacher, W. Dienst, Proc. Am. Ceram. Soc., Anaheim, California, USA, Nov. 1971.
- [21] P. Zeisser, G. Maraniello, P. Combette, J. Nucl. Mater., 65 (1977) 48.
- [22] S.L. Hayes, J.K. Thomas, K.L. Peddicord, Mat. Let., 9 (1990) 435.



Nuclear Engineering Division

Argonne National Laboratory
9700 South Cass Avenue, Bldg. 208
Argonne, IL 60439

www.anl.gov



Argonne National Laboratory is a U.S. Department of Energy
laboratory managed by UChicago Argonne, LLC